

A Bifurcation Analysis of a 3D Blowfly Model in Discrete and Continuous Time

Thorsten Hüls*

Fakultät für Mathematik

Universität Bielefeld

Postfach 100131, 33501 Bielefeld

Germany

huels@math.uni-bielefeld.de

January 23, 2008

Abstract

In this paper, we extend the two-dimensional discrete time model of the virtual fly, developed by Bøddeker and Egelhaaf in [Bøddeker & Egelhaaf, 2003], into three space dimensions, and introduce its continuous time analog. Like real blowflies, the virtual counterparts exhibit a dichotomous chasing behavior: depending on size, velocity and the course of the targets, they catch the targets or pursue them at constant distance. Here, we analyze this behavioral characteristic with respect to the course of the target, in particular, we choose trajectories, spiraling upwards. After setting up the three-dimensional model, we transform it into the local coordinates of the pursuer, using equivariance properties. Then bifurcation tools apply, and it turns out that depending on the gradient and the curvature of the spiraling trajectory, a fixed point in the transformed system can lose or gain stability. A stable fixed point corresponds in the original system to a trajectory, on which the virtual fly follows the target at constant distance. In this way, we explain the dichotomous behavior through the occurrence of bifurcations.

Keywords: Bifurcation analysis, equivariant systems, pursuit behavior of blowflies.

1 Introduction

Male blowflies chase and catch the female flies in the context of mating behavior on virtuous trajectories. These high speed chases require a fast, visually guided control system, cf. [Land & Collett, 1974]. The question arises, how these insects are able to control their

*Supported by the Research Center for Mathematical Modelling (FSPM), Bielefeld University.

artistic movements. In order to understand the underlying control mechanism, biological experiments are performed in which the female fly was replaced by a black ball, see [Collett & Land, 1978, Böddeker et al., 2003], that moves on a circular trajectory. As it turns out, male flies still chase these targets and, depending on size and velocity, they either pursue the targets at a nearly constant distance or they follow an oscillatory or even chaotic trajectory that enables them to catch the target. This leads to the question, whether explicit decision making is needed to generate the observed dichotomous behavior or if these characteristics are generated automatically by the dynamics of the control mechanism.

For finding an answer, the model of the virtual fly was developed by Böddeker and Egelhaaf in [Böddeker & Egelhaaf, 2003, Böddeker & Egelhaaf, 2005]. This model was constructed in two space dimensions, since biological experiments showed that male blowflies tend to fly in planes parallel to the circular trajectory of the target.

The mathematical equivalent of the observed change of behavior from catching to chasing is a bifurcation, and bifurcation theory enables the detection of critical parameter values, where the dynamics of the system changes structurally, see [Kuznetsov, 2004, Wiggins, 2003]. In [Hüls, 2005], this powerful tool is applied to the two-dimensional model of the virtual fly. As it turns out, some simple control mechanisms are capable of generating the dichotomous behavior. Therefore explicit decision making is not needed to explain the observed characteristics.

Though the experimental setup favors two dimensional trajectories, it is clear that real trajectories of female blowflies are truly three-dimensional. Therefore we extend in this paper the model of the virtual fly to three space dimensions and analyze whether this still supports dichotomous behavior. This generalization is introduced in Sec. 2. We put special emphasis on the fact that it should reproduce the two-dimensional results, when the movement is restricted to the two-dimensional xy -plane.

For the forthcoming analysis, it is essential to eliminate a common movement of the system. Formally, we transform the model, written in global coordinates, into the local coordinates of the pursuer, using equivariant transformations. We first translate the position of the pursuer to the origin and by two rotations in xy - and xz -direction, we fix its orientation to the x -axis. As it turns out, these transformations are quite involved, since rotation matrices in xy and xz -direction do not commute. Alternatively, one can interpret this approach as follows: In each time step, a comoving coordinate system is introduced in which position and orientation of the pursuer is fixed. Note that this ansatz works for general trajectories of the target and is thus more general than the ansatz, proposed in [Hüls, 2005], that only works for linear and circular trajectories, respectively. We refer to the transformed system as frozen system, cf. [Beyn & Thümmel, 2004] where equivariant transformations are applied to PDEs, exhibiting traveling wave or spiral solutions.

In [Hüls, 2005], depending on velocity and size of the target, the occurrence of rigid trajectories on which the pursuer follows the target at constant distance was analyzed. Obviously, also the chosen course of the target influences the success of catching. As a prototype we take trajectories, spiraling upwards, where parameters are curvature and gradient. Then, a stable fixed point of the frozen system corresponds to a trajectory, on which the pursuer follows the target at constant distance. Varying parameters, the fixed point may lose its stability. We detect these changes of stability, using bifurcation tools cf. [Dhooge et al., 2003].

Note that male flies cannot follow unstable trajectories. Therefore, they will switch to other stable objects like periodic orbits or invariant curves. Doing so, they will probably meet and catch the target.

In Sec. 3 we introduce the continuous time analog of this model and transform it into local coordinates, using the techniques from Sec. 2. The model exhibits the same type of bifurcations, but at slightly different parameters. The bifurcation toolbox MATCONT, see [Dhooge et al., 2003], supports for continuous time systems numerical branch switching from equilibria to periodic orbits, occurring via Hopf-bifurcations. Although these curves exist for the discrete time model as well, we only shown them in continuous time.

2 A 3D model of the virtual fly in discrete time

In [Böddeker & Egelhaaf, 2003, Böddeker & Egelhaaf, 2005, Böddeker et al., 2003] the two-dimensional model of the virtual fly was developed by Böddeker and Egelhaaf, and its dynamics were analyzed in [Hüls, 2005].

In this section, we first revisit this two-dimensional model, and introduce an extension into three space dimensions. Doing so, we gain a model that describes the positions of the male fly and of the target in global coordinates with some additional internal coordinates. For the analysis, it is useful to transform the system into the local coordinates of the male fly, see Sec. 2.3.

As an example, we analyze a three-dimensional trajectory, spiraling upwards. The critical parameters are the gradient and the curvature of these trajectories. We detect parameter regions, using bifurcation tools cf. [Dhooge et al., 2003], for which stable fixed points in the transformed system exist. These fixed points correspond to rigid trajectories, on which the male fly follows the target at constant distance.

2.1 The 2D model of the virtual fly revisited

The two-dimensional model, see [Hüls, 2005] has seven state variables $Y = (s, a, \sigma, v, x, z, \beta)^T$ as illustrated in Fig. 1. The dynamics can be written as follows

$$Y_{n+1} = f(Y_n), \quad n \in \mathbb{N},$$

where

$$f \begin{pmatrix} s \\ a \\ \sigma \\ v \\ x \\ z \\ \beta \end{pmatrix} = \begin{pmatrix} \frac{1}{1+T_s} \left(\rho(x, z, T) S_v e^{\frac{-\rho(x, z, T)}{q}} + S_m + T_s s \right) \\ \frac{1}{1+T_a} (G \sin(\theta(z-x) - \sigma) + T_a a) \\ \sigma + a \\ (1-M)v + MsD_\sigma \begin{pmatrix} 1 \\ 0 \end{pmatrix} \\ x + v \\ z + \ell D_\beta \begin{pmatrix} 1 \\ 0 \end{pmatrix} \\ \beta + \varphi \end{pmatrix}. \quad (1)$$

parameter	value	dim.	interpretation
T	3 – 15	mm	size of the target
S_m	0.8	m/s	minimal speed of the fly
G	0.125	1	describes the gain of the orientation change
T_s	80	1	parameter for a low-pass filter, realizing a neuronal reaction time for speed control
T_a	15	1	parameter for a low-pass filter, realizing a neuronal reaction time for target fixation
q	0.0865	1	parameter for speed control
S_v	67	m/s	parameter for speed control
M	0.0455	1	kinematic constant

Table 1: *Parameters and their typical settings in the model of the virtual fly.*

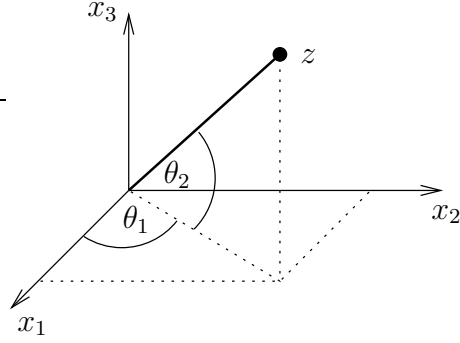


Figure 2: *Illustration of the Euclidean angles $\theta_{1,2}$.*

where

$$F \begin{pmatrix} s \\ a^1 \\ a^2 \\ \sigma^1 \\ \sigma^2 \\ v \\ x \\ z \\ \beta^1 \\ \beta^2 \end{pmatrix} = \begin{pmatrix} \frac{1}{1+T_s} (\rho(x, z, T) S_v e^{-\rho(x, z, T)/q} + S_m + T_s s) \\ \frac{1}{1+T_{a^1}} (G \sin(\theta_1 (D_{13}(-\sigma^2) D_{12}(-\sigma^1) (z - x))) + T_{a^1} a^1) \\ \frac{1}{1+T_{a^2}} (G \sin(\theta_2 (D_{13}(-\sigma^2) D_{12}(-\sigma^1) (z - x))) + T_{a^2} a^2) \\ \sigma^1 + a^1 \\ \sigma^2 + a^2 \\ (1 - M)v + Ms D_{12}(\sigma^1) D_{13}(\sigma^2) \begin{pmatrix} 1 \\ 0 \\ 0 \end{pmatrix} \\ x + v \\ z + \ell D_{12}(\beta^1) D_{13}(\beta^2) \begin{pmatrix} 1 \\ 0 \\ 0 \end{pmatrix} \\ \beta^1 + \varphi^1 \\ \beta^2 + \varphi^2 \end{pmatrix}. \quad (5)$$

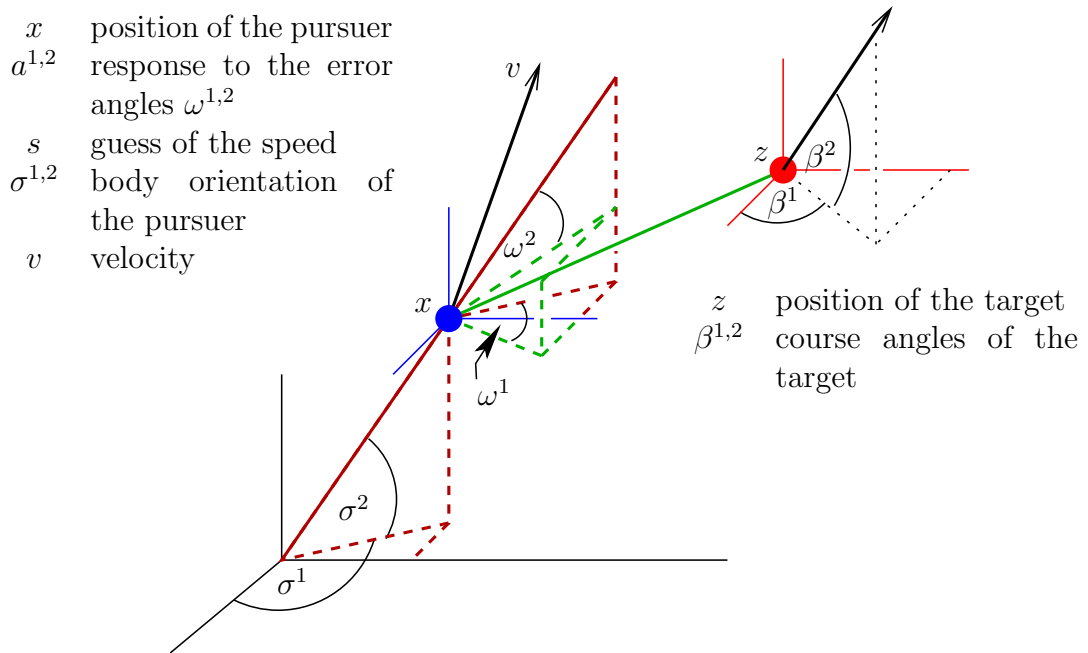


Figure 3: *Settings in the three-dimensional model of the virtual fly.*

Here ℓ , φ^1 and φ^2 are external variables that determine the velocity and the course of the target and may depend on time. D_{12} and D_{13} are rotations around the x_3 - and the x_2 -axis, respectively, which are formally defined as

$$D_{12}(\varphi) = \begin{pmatrix} \cos \varphi & -\sin \varphi & 0 \\ \sin \varphi & \cos \varphi & 0 \\ 0 & 0 & 1 \end{pmatrix}, \quad D_{13}(\varphi) = \begin{pmatrix} \cos \varphi & 0 & -\sin \varphi \\ 0 & 1 & 0 \\ \sin \varphi & 0 & \cos \varphi \end{pmatrix}.$$

The functions θ_1 and θ_2 compute the angle of a vector $z \in \mathbb{R}^3$ w.r.t. the (x_1, x_3) - and the (x_1, x_2) -planes, cf. Fig. 2 :

$$\theta_1(z) = \theta \begin{pmatrix} z_1 \\ z_2 \end{pmatrix}, \quad \theta_2(z) = \theta \begin{pmatrix} (D_{12}(-\theta_1(z))z)_1 \\ (D_{12}(-\theta_1(z))z)_3 \end{pmatrix}$$

with $\theta(y)$ as in Eq. (3). Since error angles in left-right and up-down direction are computed separately, we introduce two constants T_{a1} and T_{a2} for the corresponding low-pass filters to realize (possibly different) neuronal reaction times in left-right and up-down direction. Since different values for these parameters are not known from experiments, we take $T_{a1} = T_{a2} = T_a = 15$.

2.2.1 Invariant planes

The three-dimensional model exhibits several planes in \mathbb{R}^3 that are invariant for specific values of the internal variables, see Fig. 4.

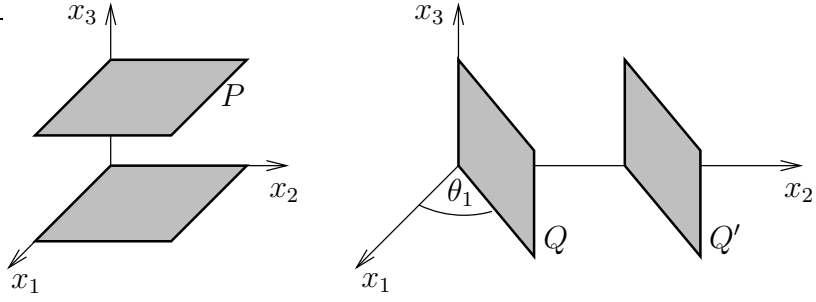


Figure 4: *Invariant planes in the three-dimensional model of the virtual fly.*

If, for example, x and z in (5) are restricted to a plane P that is parallel to the (x_1, x_2) -plane, v lies in the (x_1, x_2) -plane and additionally $0 = a^2 = \sigma^2 = \beta^2$ hold, then the v -component of $F(s, a^1, 0, \sigma^1, 0, v, x, z, \beta^1, 0)$ lies in the (x_1, x_2) -plane while the x and z components lie in P . In this sense, the plane P is invariant (left of Fig. 4).

On the other hand, the plane Q' having the angle θ_1 w.r.t. the x_1 -axis, cf. the right of Fig. 4, is invariant in the following sense: For $x, z \in Q'$, $v \in Q$ and $a^1 = 0$, $\sigma^1 = \beta^1 = \theta_1$, the image under F lies in the same areas.

From the first invariance, we conclude that the three-dimensional model is a natural extension of the two-dimensional one, since it generates (see Proposition 1) the same trajectories, under the restrictions given above.

Proposition 1 *Let $T_a = T_{a^1}$, $\beta = \beta^1$, $\varphi^2 = 0$ and for a given $\gamma \in \mathbb{R}$ let*

$$X^2 = \begin{pmatrix} s & a^1 & \sigma^1 & \begin{pmatrix} v_1 \\ v_2 \end{pmatrix} & \begin{pmatrix} x_1 \\ x_2 \end{pmatrix} & \begin{pmatrix} z_1 \\ z_2 \end{pmatrix} & \beta^1 \end{pmatrix},$$

$$X^3 = \begin{pmatrix} s & a^1 & 0 & \sigma^1 & 0 & \begin{pmatrix} v_1 \\ v_2 \\ 0 \end{pmatrix} & \begin{pmatrix} x_1 \\ x_2 \\ \gamma \end{pmatrix} & \begin{pmatrix} z_1 \\ z_2 \\ \gamma \end{pmatrix} & \beta^1 & 0 \end{pmatrix}.$$

Then

$$F(X^3) = \begin{pmatrix} f^s(X^2) \\ f^a(X^2) \\ 0 \\ f^\sigma(X^2) \\ 0 \\ f^v(X^2) \\ 0 \\ f^x(X^2) \\ \gamma \\ f^z(X^2) \\ \gamma \\ f^\beta(X^2) \\ 0 \end{pmatrix}.$$

Proof: It holds that

$$\rho \left(\begin{pmatrix} x_1 \\ x_2 \\ \gamma \end{pmatrix}, \begin{pmatrix} z_1 \\ z_2 \\ \gamma \end{pmatrix}, T \right) = \rho \left(\begin{pmatrix} x_1 \\ x_2 \end{pmatrix}, \begin{pmatrix} z_1 \\ z_2 \end{pmatrix}, T \right)$$

and therefore $F^s(X^3) = f^s(X^2)$. Since

$$\begin{aligned} \theta_1(D_{13}(0)D_{12}(-\sigma^1)(z-x)) &= \theta \begin{pmatrix} (z-x)_1 \\ (z-x)_2 \end{pmatrix} - \sigma^1, \\ \theta_2((D_{13}(0)D_{12}(-\sigma^1)(z-x)) &= 0 \end{aligned}$$

we get $F^{a^1}(X^3) = f^a(X^2)$ and $F^{a^2}(X^3) = 0$.

Furthermore, $F^v(X^3)_3 = 0$ since $\sigma^2 = 0$ and as a consequence $F^x(X^3)_3 = \gamma$. Finally, it follows from $\beta^2 = 0$ that $F^z(X^3)_3 = \gamma$. ■

2.3 Transformation into local coordinates

The model (5) of the virtual fly is formulated in global coordinates in \mathbb{R}^3 (with additional internal coordinates). We analyze the existence of stable rigid trajectories, on which the male fly pursues the target at constant distance. For the target, we choose a three-dimensional trajectory that spirals upwards, see Fig. 5. In this case, the dynamics cannot be reduced to one of the invariant planes. However, we will show that, after suitable transformations, the system is still amenable to bifurcation analysis.

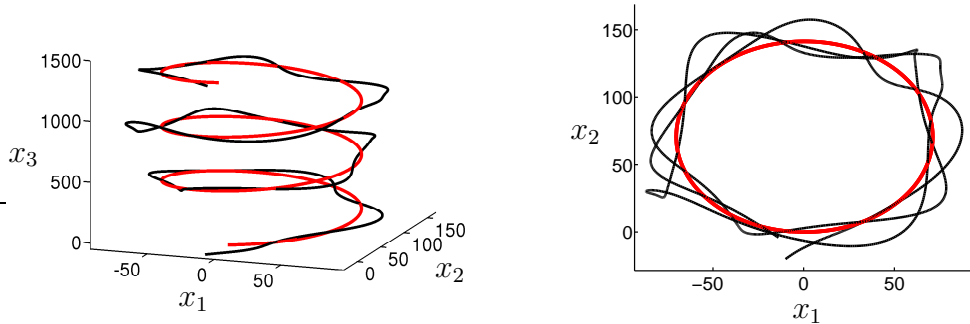


Figure 5: 1500 iterates of (5) for $T = 8$, $\ell = 1.25$, $\varphi^1 = 0.0125$, $\varphi^2 = 0$, $\beta_2 = \frac{\pi}{4}$. The trajectories of the target (in red) and of the pursuer (in black) are shown. The projection onto the (x_1, x_2) -plane is given in the right diagram.

For the forthcoming analysis, it is essential to transform the system into the local coordinates of the pursuer. In the transformed system, the position x of the pursuer is the origin and the heading is the direction of the x_1 -axis, i.e. $\sigma^1 = \sigma^2 = 0$. We will call this the

frozen form. Note that this goal can also be achieved by fixing the position of the target z , cf. [Hüls, 2005].

Let

$$X = (s \ a^1 \ a^2 \ \sigma^1 \ \sigma^2 \ v \ x \ z \ \beta^1 \ \beta^2)^T.$$

The system (5) is transformed in the following three steps. First, the position of the pursuer x is shifted to zero. Then the rotation σ^1 of the body w.r.t. the (x_1, x_2) -plane is compensated and finally, the rotation σ^2 is corrected. As a consequence, the target takes over the movement of the pursuer in this coordinate system.

In the first step, we carry out simultaneous translations of x and z . Define the special translation Γ_1 by

$$\Gamma_1(\delta)X = X + (0 \ 0 \ 0 \ 0 \ 0 \ 0 \ \delta \ \delta \ 0 \ 0)^T, \quad (6)$$

then the equivariance relation, see Appendix A,

$$F(\Gamma_1(\delta)X) = \Gamma_1(\delta)F(X)$$

holds. Transforming to the variables $Y = \Gamma_1(-v)X$ (cf. Appendix A, Proposition 2) we see that the x -variable stays at 0 if $x_0 = 0$. Hence it is sufficient to write the dynamics in terms of the reduced set of variables

$$\tilde{X} = (s \ a^1 \ a^2 \ \sigma^1 \ \sigma^2 \ v \ z \ \beta^1 \ \beta^2)^T$$

as follows

$$\tilde{F}(\tilde{X}) = \begin{pmatrix} \frac{1}{1+T_s} (\rho(0, z, T)S_v e^{-\rho(0, z, T)/q} + S_m + T_s s) \\ \frac{1}{1+T_{a^1}} (G \sin(\theta_1(D_{13}(-\sigma^2)D_{12}(-\sigma^1)z)) + T_{a^1} a^1) \\ \frac{1}{1+T_{a^2}} (G \sin(\theta_2(D_{13}(-\sigma^2)D_{12}(-\sigma^1)z)) + T_{a^2} a^2) \\ \sigma^1 + a^1 \\ \sigma^2 + a^2 \\ (1 - M)v + MsD_{12}(\sigma^1)D_{13}(\sigma^2) \begin{pmatrix} 1 \\ 0 \\ 0 \end{pmatrix} \\ z + \ell D_{12}(\beta^1)D_{13}(\beta^2) \begin{pmatrix} 1 \\ 0 \\ 0 \end{pmatrix} - v \\ \beta^1 + \varphi^1 \\ \beta^2 + \varphi^2 \end{pmatrix}. \quad (7)$$

For the initial value $\sigma_0^2 = 0$, the iterates σ_n^2 stay zero. Eliminating the σ^2 variable and including (13), we finally arrive at

$$\begin{pmatrix} s_{n+1} \\ a_{n+1}^1 \\ a_{n+1}^2 \\ v_{n+1} \\ z_{n+1} \\ \beta_{n+1}^1 \\ \beta_{n+1}^2 \\ \alpha_{n+1} \end{pmatrix} = \begin{pmatrix} \frac{1}{1+T_s} (\rho(0, z_n, T) S_v e^{-\rho(0, z_n, T)/q} + S_m + T_s s_n) \\ \frac{1}{1+T_{a^1}} (G \sin(\theta_1(z_n)) + T_{a^1} a_n^1) \\ \frac{1}{1+T_{a^2}} (G \sin(\theta_2(z_n)) + T_{a^2} a_n^2) \\ D_{13}(-a_n^2) D_{13}(-\alpha_n) D_{12}(-a_n^1) D_{13}(\alpha_n) \left((1-M)v_n + Ms \begin{pmatrix} 1 \\ 0 \\ 0 \end{pmatrix} \right) \\ D_{13}(-a_n^2) D_{13}(-\alpha_n) D_{12}(-a_n^1) \\ \cdot \left(D_{13}(\alpha_n) z_n + \ell D_{12}(\beta_n^1) D_{13}(\beta_n^2) \begin{pmatrix} 1 \\ 0 \\ 0 \end{pmatrix} - D_{13}(\alpha_n) v_n \right) \\ \beta_n^1 + \varphi^1 - a_n^1 \\ \beta_n^2 + \varphi^2 \\ a_n^2 + \alpha_n \end{pmatrix}. \quad (15)$$

2.4 A 2D frozen model in discrete time

We find the frozen form of the two-dimensional model (1) by reducing the model from Sec. 2.3 to the (x_1, x_2) -plane. Choose $T_a = T_{a^1}$, $\beta = \beta_1$, and $0 = \varphi^2 = a^2 = v_3 = z_3$ in the three-dimensional model. By Proposition 1, movement in x_3 -direction cannot occur and consequently, the last transformation from (9) to (15) which compensates this movement, is not needed. Thus, we get the frozen form of (1) by inserting the values from above into (9):

$$\begin{pmatrix} s \\ a \\ v \\ z \\ \beta \end{pmatrix} \mapsto \begin{pmatrix} \frac{1}{1+T_s} (\rho(0, z, T) S_v e^{-\frac{\rho(z, T)}{q}} + S_m + T_s s) \\ \frac{1}{1+T_a} (G \sin(\theta(z)) + T_a a) \\ D_{-a} \left((1-M)v + Ms \begin{pmatrix} 1 \\ 0 \end{pmatrix} \right) \\ D_{-a} \left(z + \ell D_\beta \begin{pmatrix} 1 \\ 0 \end{pmatrix} - v \right) \\ \beta + \varphi - a \end{pmatrix}. \quad (16)$$

Note that due to our construction, linear trajectories as well as circular trajectories are transformed for time-independent parameters φ , ℓ into fixed points. This generalizes the approach, proposed in [Hüls, 2005], where linear and circular trajectories are treated separately.

2.5 Analysis of three-dimensional trajectories

The transformation of the system of the virtual fly into a frozen form, enables a formal analysis of the dichotomous behavior, whether the pursuer catches the target or follows it at constant distance. This change of behavior depends on the size and on the velocity (see

[Hüls, 2005]) as well as on the chosen trajectory of the target. We analyze the latter dependence, using bifurcation tools, see [Dhooge et al., 2003, Kuznetsov, 2004, Wiggins, 2003]. For the forthcoming computations, we fix the speed of the target by choosing $\ell = 1.25$.

Here, we only consider targets on trajectories, spiralling upwards. In Fig. 6, 1500 iterates, with same initial value, of the original system (5) and of the transformed systems (9) and (15) are shown.

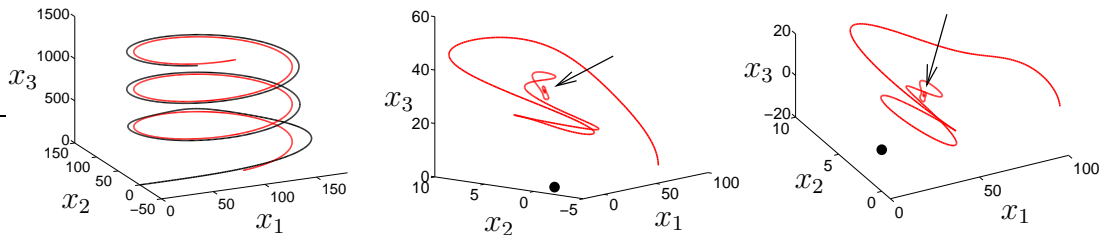


Figure 6: 1500 iterates of (5) for $T = 15$, $\ell = 1.25$, $\varphi^1 = 0.0125$, $\varphi^2 = 0$, $\beta^2 = \frac{\pi}{4}$. The trajectories of the target (in red) and the trajectory or fixed position of the pursuer (in black) are shown for the original system (left), (9) (middle) and (15) (right). The arrows indicate the position of fixed points in the frozen systems.

As one can see, a rigid trajectory on which the pursuer follows the target at constant distance (left diagram) corresponds to a fixed point in (9) as well as in (15). Note that we choose $\varphi^2 = 0$ and as a consequence, see (9), the course of the target in x_3 -direction is linear. In this special case, only the first two transformations are necessary, in order to transform rigid trajectories (Fig. 6, left), into fixed points (Fig. 6, middle).

From the construction of our model (5), one sees that φ^1 influences the curvature of the trajectory of the target, while β^2 defines its gradient. We show that for certain values of these two parameters, stable fixed points of (9) exist, that correspond to rigid trajectories in the original system (5). For a fixed size $T = 7.5$, we choose $\beta^2 = 0.1$ and continue the fixed points of (9) w.r.t. the parameter φ^1 . Fig. 7 shows the resulting bifurcation diagram, where stable fixed points are black, while unstable fixed points are plotted in red. The change of stability is caused by Neimark-Sacker bifurcations (NS), cf. [Kuznetsov, 2004, Wiggins, 2003], which are the discrete time analog of Hopf bifurcations in continuous time systems. Also fold- or limit point bifurcations (LP) occur, but only for fixed points that are already unstable. The bifurcation diagrams, shown in this article are computed, using the bifurcation toolbox MATCONT, see [Dhooge et al., 2003].

At Neimark-Sacker bifurcations, stable invariant curves are born. The computation of these curves in discrete time systems is quite involved and not supported by the current version of MATCONT. In Sec. 3, we introduce a continuous time model of the virtual fly, exhibiting the same type of bifurcations at slightly different parameters. For continuous time systems MATCONT supports the computation of invariant curves, i.e. periodic orbits, see Sec. 3.3, Fig. 12.

The bifurcation diagram in Fig. 7 depends strongly on the chosen target size T . For

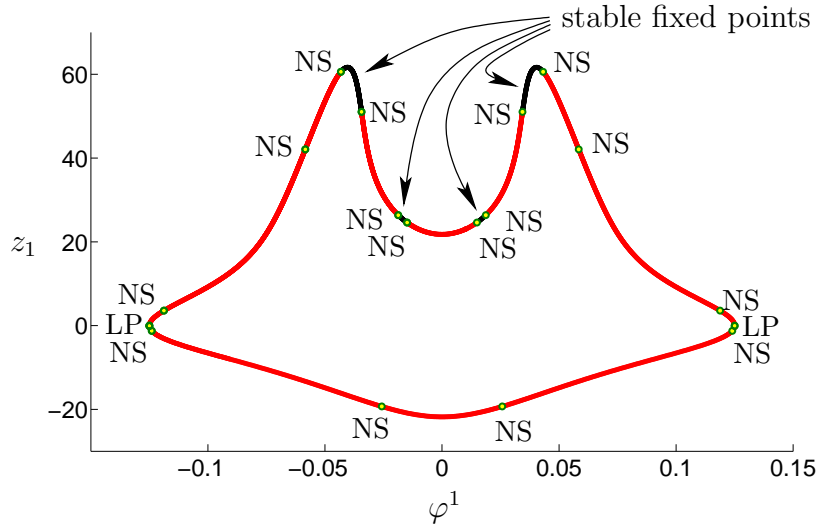


Figure 7: Continuation of fixed points for fixed $T = 7.5$, $\beta^2 = 0.1$ w.r.t. the parameter φ^1 . A black line indicates stable and a red line unstable fixed points.

$T \in \{5, 8, 8.1, 9\}$, parts of the corresponding bifurcation diagrams are plotted in the upper part of Figs. 8 and 9. A refined picture of the dependence on the target size T is given in Fig. 10, where these bifurcation diagrams are plotted in 3D for $T \in [3, 13]$.

In a second computation, the Neimark-Sacker bifurcations, by which the fixed points gain or lose stability, are continued w.r.t. the parameters φ^1 and β^2 . Doing so, we find regions in the (φ^1, β^2) -parameter plane, where stable fixed points exist. These computations are illustrated in the lower diagrams of Figs. 8 and 9. For parameter values in the stable regions, marked with \textcircled{S} , a rigid trajectory exists for the original system (5), on which the pursuer follows the target at constant distance. In the complementary areas, the numerical computations from Sec. 3 suggest that there exist stable invariant curves. The way, these curves influence the behavior of the pursuer is discussed in Sec. 3.

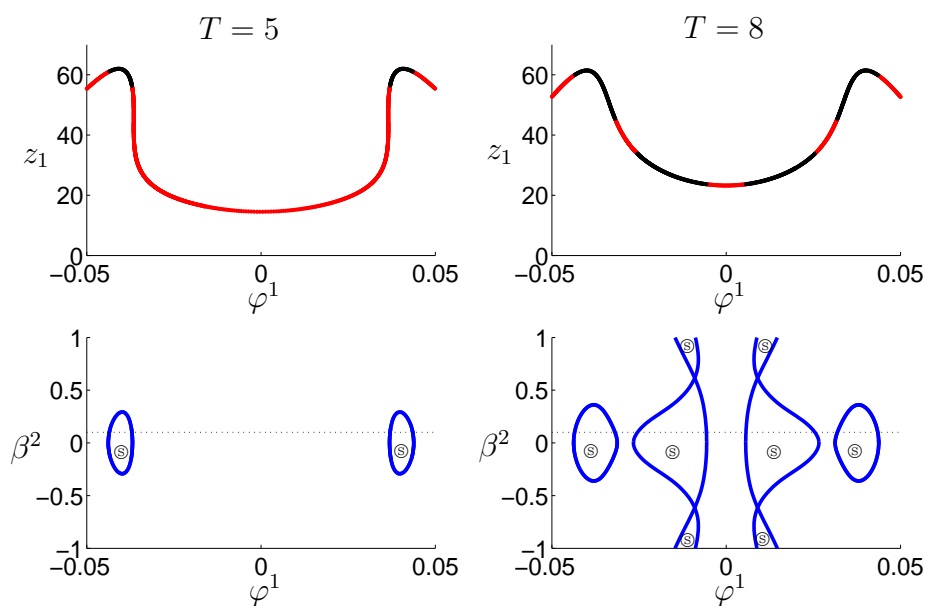


Figure 8: The upper diagrams show the continuation of fixed points w.r.t. the parameter φ^1 for fixed $\beta^2 = 0.1$, $T = 5$ (left) and $T = 8$ (right). The change of stability (red: unstable, black: stable) is caused by Neimark-Sacker bifurcations, cf. Fig. 7. The continuation of Neimark-Sacker bifurcations w.r.t. the parameters φ^1 and β^2 is shown in the lower diagrams. Regions in which stable fixed points exist have been marked with \textcircled{S} .

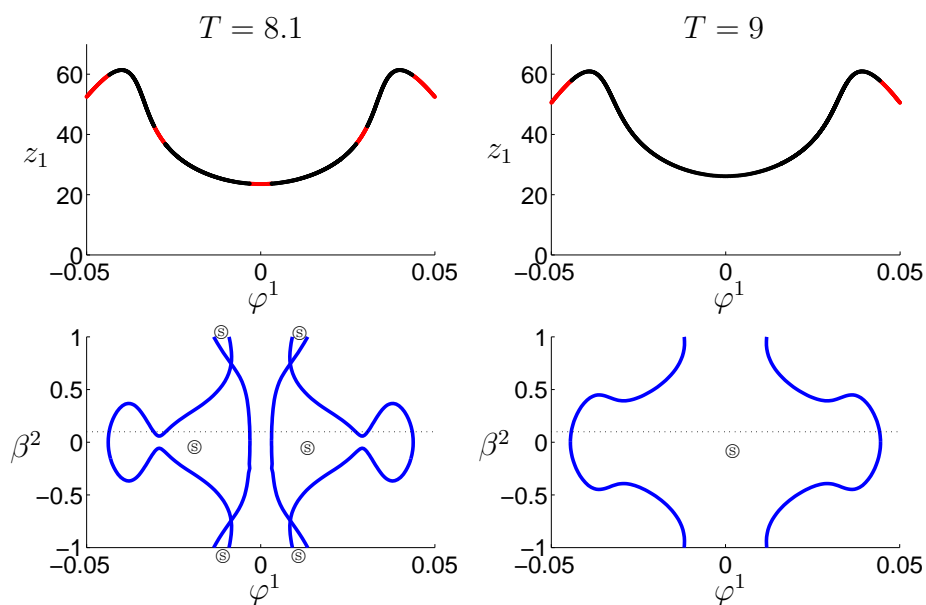


Figure 9: The same illustration as in Fig. 8 for $T = 8.1$ (left) and $T = 9$ (right).

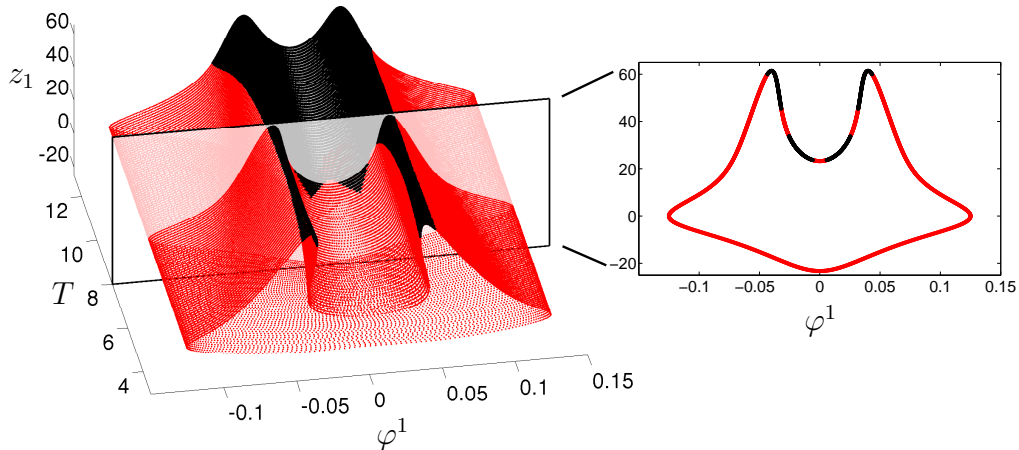


Figure 10: *Bifurcation diagram for fixed $\beta^2 = 0.1$, cf. Fig. 7, with $T \in [3, 13]$. Stable and unstable fixed points are plotted in black and red, respectively. The diagram on the plane $T = 8$ is separately drawn (right).*

3 A continuous time model of the virtual fly

In this section, we introduce a continuous time version of the virtual fly that is modelled after the discrete time system, introduced in Sec. 2. A bifurcation analysis for this model shows the same phenomena that we already observed in the discrete time model at slightly different parameter values. We illustrate this by computing the bifurcation diagram from Fig. 10 also for the continuous time model. Note that it is well known, see e.g. [Hofbauer & Iooss, 1984], that Hopf bifurcations in continuous time systems lead under discretization to Neimark-Sacker bifurcations, where the value of the bifurcation parameter changes slightly.

The computation of periodic orbits that emerge from Hopf bifurcations is for continuous time systems supported by MATCONT, cf. [Dhooge et al., 2003]. The corresponding pictures are given in Sec. 3.3. We indicate the relevance of these periodic orbits on the behavior of the pursuer.

3.1 Setup of the model

First, we apply the first order low-pass filter $U'_0 = \frac{1}{\tau}(U_I - U_0)$ with the setting $\tau = T_s$, $U_0 = s$, $U_I = \rho(x, z, T)S_v e^{-\rho(x, z, T)/q} + S_m$ and get

$$s' = \frac{1}{T_s} (\rho(x, z, T)S_v e^{-\rho(x, z, T)/q} + S_m - s).$$

The error angles a^1 , a^2 are defined as (see [Hüls, 2005] for more details)

$$\begin{aligned}(a^1)' &= \frac{1}{T_{a^1}} (G \sin(\theta_1(D_{13}(-\sigma^2)D_{12}(-\sigma^1)(z-x))) - a^1), \\ (a^2)' &= \frac{1}{T_{a^2}} (G \sin(\theta_2(D_{13}(-\sigma^2)D_{12}(-\sigma^1)(z-x))) - a^2).\end{aligned}$$

The remaining equations are constructed, such that a discretization with the explicit Euler-method with step-size 1 leads to the discrete time system (5). The resulting continuous time model of the virtual fly is:

$$\begin{pmatrix} s \\ a^1 \\ a^2 \\ \sigma^1 \\ \sigma^2 \\ v \\ x \\ z \\ \beta^1 \\ \beta^2 \end{pmatrix}' = \begin{pmatrix} \frac{1}{T_s} (\rho(x, z, T)S_v e^{-\rho(x,z,T)/q} + S_m - s) \\ \frac{1}{T_{a^1}} (G \sin(\theta_1(D_{13}(-\sigma^2)D_{12}(-\sigma^1)(z-x))) - a^1) \\ \frac{1}{T_{a^2}} (G \sin(\theta_2(D_{13}(-\sigma^2)D_{12}(-\sigma^1)(z-x))) - a^2) \\ a^1 \\ a^2 \\ M \begin{pmatrix} -v + sD_{12}(\sigma^1)D_{13}(\sigma^2) \\ \begin{pmatrix} 1 \\ 0 \\ 0 \end{pmatrix} \end{pmatrix} \\ v \\ \ell D_{12}(\beta^1)D_{13}(\beta^2) \begin{pmatrix} 1 \\ 0 \\ 0 \end{pmatrix} \\ \varphi^1 \\ \varphi^2 \end{pmatrix}. \quad (17)$$

3.2 Transformation into local coordinates

As in the discrete time case, we transform (17) in three steps into local coordinates. The first two steps are equivariant transformations with the same operators Γ_1 , Γ_2 , defined in (6) and (8). The resulting system in the reduced set of variables

$$\bar{X} = (s, a^1, a^2, \sigma^2, v, z, \beta^1, \beta^2)^T,$$

which corresponds to (9), has the form

$$\begin{pmatrix} s \\ a^1 \\ a^2 \\ \sigma^2 \\ v \\ z \\ \beta^1 \\ \beta^2 \end{pmatrix}' = \begin{pmatrix} \frac{1}{T_s} (\rho(0, z, T) S_v e^{-\rho(0, z, T)/q} + S_m - s) \\ \frac{1}{T_{a^1}} (G \sin(\theta_1(D_{13}(-\sigma^2)z)) - a^1) \\ \frac{1}{T_{a^2}} (G \sin(\theta_2(D_{13}(-\sigma^2)z)) - a^2) \\ a^2 \\ M \begin{pmatrix} -v + s D_{13}(\sigma^2) \begin{pmatrix} 1 \\ 0 \\ 0 \end{pmatrix} \end{pmatrix} - a^1 L_{12} v \\ \ell D_{12}(\beta^1) D_{13}(\beta^2) \begin{pmatrix} 1 \\ 0 \\ 0 \end{pmatrix} - v - a^1 L_{12} z \\ \varphi^1 - a^1 \\ \varphi^2 \end{pmatrix}, \quad (18)$$

where

$$L_{12} = \begin{pmatrix} 0 & -1 & 0 \\ 1 & 0 & 0 \\ 0 & 0 & 0 \end{pmatrix}, \quad L_{13} = \begin{pmatrix} 0 & 0 & -1 \\ 0 & 0 & 0 \\ 1 & 0 & 0 \end{pmatrix}.$$

In the third step, we define the change of variables $\bar{Y} = \Gamma_3(-\alpha)\bar{X}$, with Γ_3 as in (10). If α satisfies $\alpha' = a^2$, we finally get the system

$$\begin{pmatrix} s \\ a^1 \\ a^2 \\ v \\ z \\ \beta^1 \\ \beta^2 \\ \alpha \end{pmatrix}' = \begin{pmatrix} \frac{1}{T_s} (\rho(0, z, T) S_v e^{-\rho(0, z, T)/q} + S_m - s) \\ \frac{1}{T_{a^1}} (G \sin(\theta_1(z)) - a^1) \\ \frac{1}{T_{a^2}} (G \sin(\theta_2(z)) - a^2) \\ M \begin{pmatrix} -v + s \begin{pmatrix} 1 \\ 0 \\ 0 \end{pmatrix} \end{pmatrix} - a^1 D_{13}(-\alpha) L_{12} D_{13}(\alpha) v - a^2 L_{13} v \\ D_{13}(-\alpha) \ell D_{12}(\beta^1) D_{13}(\beta^2) \begin{pmatrix} 1 \\ 0 \\ 0 \end{pmatrix} - v - a^1 D_{13}(-\alpha) L_{12} D_{13}(\alpha) z - a^2 L_{13} z \\ \varphi^1 - a^1 \\ \varphi^2 \\ a^2 \end{pmatrix},$$

which is the continuous time equivalent of (15).

3.3 Analysis of three-dimensional trajectories

The analysis of upwards spiralling trajectories of the target gives similar results to the one, introduced in Sec. 2.5 for the discrete time case.

A bifurcation diagram for fixed $\beta^2 = 0.1$, $T \in [3, 13]$ w.r.t. the parameter φ^1 , see Fig. 10, exhibits the same type of bifurcations as in the continuous time case. Comparing Figs.

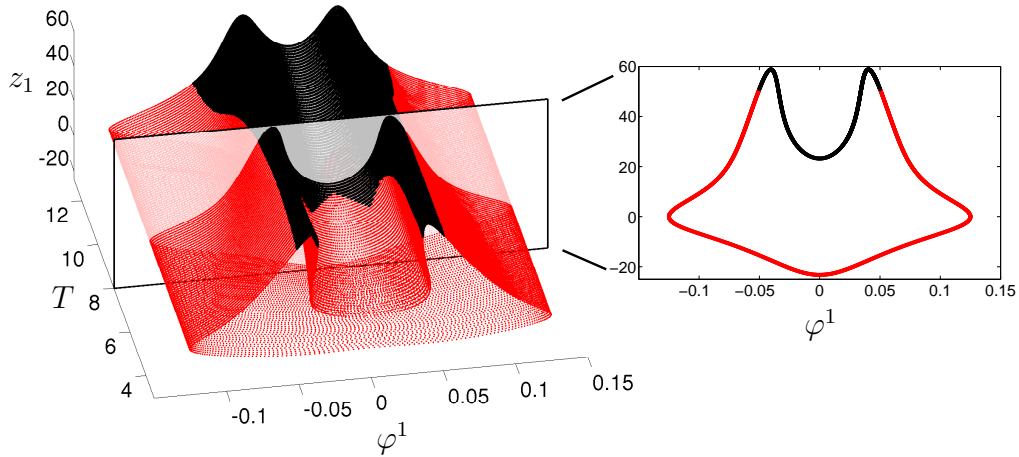


Figure 11: *Bifurcation diagram for fixed $\beta^2 = 0.1$ with $T \in [3, 13]$. Stable and unstable equilibria are plotted in black and red, respectively. The diagram on the plane $T = 8$ is separately drawn (right).*

10 and 11, one sees that the value of the parameter T , where these bifurcations occur in discrete and continuous time, is slightly shifted.

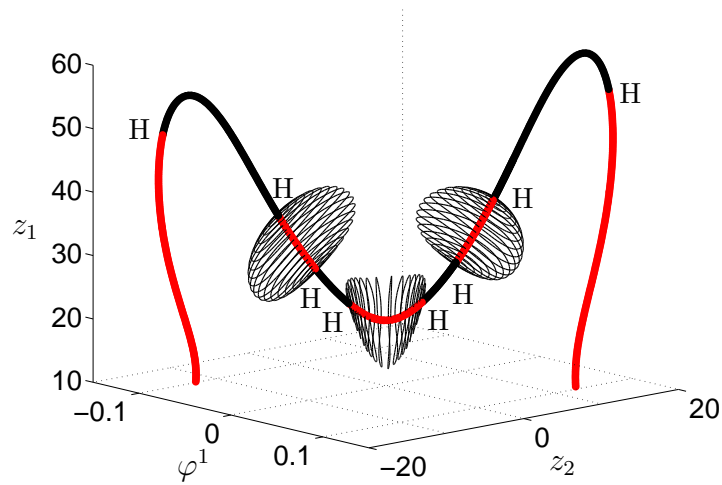


Figure 12: *Continuation of equilibria for fixed $T = 7$, $\beta^2 = 0.1$ w.r.t. the parameter φ^1 , cf. Fig. 7. The periodic orbits that are born at Hopf bifurcations (H) are also shown. Stable and unstable objects are plotted in black and red, respectively.*

In Fig. 12, the continuous time version of Fig. 7 is given, where periodic orbits that emerge from Hopf bifurcations are also displayed. Note that these orbits take over the stability, the

black equilibria lose at Hopf bifurcations. Periodic orbits lead to trajectories in the original system, on which the male fly pursues the target at a periodically fluctuating distance, see Fig. 13.

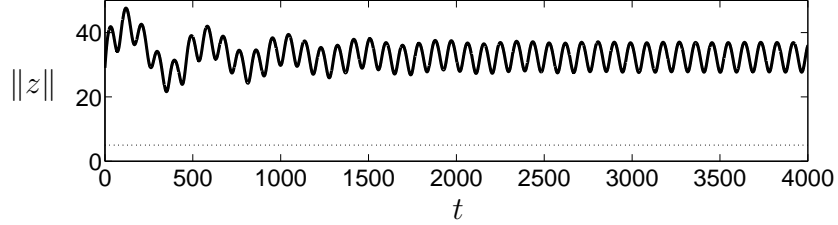


Figure 13: For $T = 7$, $\beta^2 = 0.1$, $\varphi^1 = 0.0272$ and a starting point in a neighborhood of the periodic orbit, the distance between pursuer and target, $\|z(t)\|$ in (18), is plotted over t [ms]. The dotted line denotes the catching distance.

When the fixed point or a periodic orbit lose stability at a bifurcation, the attraction to this object in a neighborhood of the bifurcation is quite weak. For parameters close to the bifurcation, the pursuer will probably meet (and catch) the target on its way to the weakly stable state.

The occurrence of these bifurcations depends strongly on the choice of the parameter T . For $T = 6.5$, see Fig. 14, the periodic orbits became much larger. Furthermore, they lose their stability via a Neimark-Sacker bifurcations (change of color from black to red).

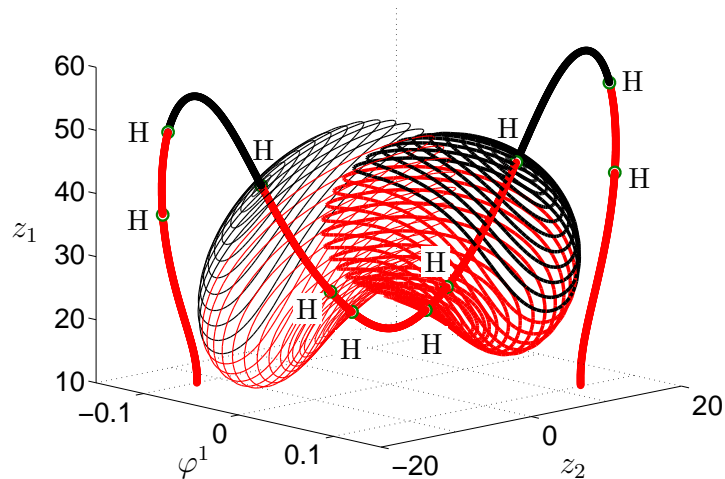


Figure 14: Continuation of equilibria and periodic orbits for fixed $T = 6.5$, $\beta^2 = 0.1$ w.r.t. the parameter φ^1 . The periodic orbits lose their stability via Neimark-Sacker bifurcations. Stable and unstable objects are plotted in black and red, respectively.

Starting close to an unstable periodic orbit, the distance between pursuer and target is shown in Fig. 15. For the chosen initial point close to the periodic orbit, the distance gets after a short time less than 5mm, which means that the pursuer catches the target. Thus for decreasing T catching instead of pursuing becomes more likely.

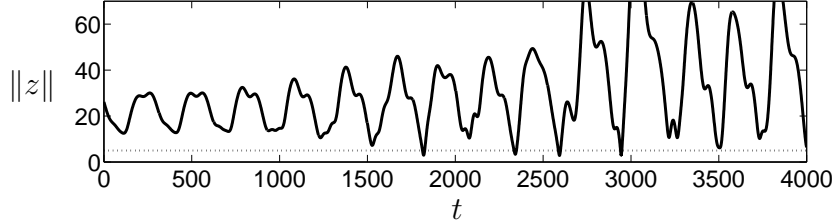


Figure 15: For $T = 6.5$, $\beta^2 = 0.1$, $\varphi^1 = 0.0163$ and a starting point close to the periodic orbit, the distance between pursuer and target, $\|z(t)\|$ in (18), is plotted over t [ms]. The dotted line denotes the catching distance.

4 Conclusion

In this paper, a three-dimensional blow-fly model is introduced in discrete as well as in continuous time. These insects exhibit a dichotomous behavior in biological experiment. Either they catch the target or pursue it at constant distance on a rigid trajectory.

After a transformation in the local coordinates of the pursuer, using equivariance properties, bifurcation tools can be applied. We put special emphasis on the influence of the course of the target on the pursuit behavior of male flies.

For upwards spiralling trajectories of the target, we analyze the existence of rigid trajectories, which correspond to stable fixed points of the frozen system. The parameters for our analysis are gradient and curvature of the trajectory of the target. Furthermore, we detect areas in the parameter plane, for which stable fixed points exist.

Note that this analysis gives only local results. The occurrence of a stable fixed point does not exclude the coexistence of other stable objects, like invariant curves or stable attractors, which do not correspond to rigid trajectories in the original system. On a periodic orbit, for example, the pursuer takes up a larger part of the space, thus catching becomes more likely. Furthermore, when the parameters in the two-parameter diagram are close to the boundary of the stable region, the attraction of the corresponding fixed point is quite weak. Therefore, it will take a long time, until this fixed point attracts the pursuer and consequently, the pursuer may catch the target on its way to this stable state.

Summarizing this, the above described analysis can only provide existence results of rigid and of time periodic trajectories in continuous time as well as of rigid and quasi-periodic trajectories in discrete time. Furthermore, the analysis shows that the simple control system of the virtual fly in 3D is capable to generate complicated dynamics. Explicit decision making is not needed in order to generate dichotomous behavior.

For our analysis, we choose regular trajectories, for which the resulting model is autonomous. The question arises, whether similar results can also be derived for more arbitrary trajectories of the target, that lead to non-autonomous dynamical systems. This is a mathematically challenging area, since notions of non-autonomous bifurcations and corresponding bifurcation results are currently under development, see for example [Langa et al., 2006, Rasmussen, 2006, Hüls, 2007].

Acknowledgment

The author is grateful to Lukas Sowa for extensive work on the bifurcation diagrams. The author thanks Wolf-Jürgen Beyn for very helpful discussions about this article.

Appendix A Equivariant dynamical systems

Consider the discrete time dynamical system

$$x_{n+1} = F(x_n), \quad n \in \mathbb{N} \quad (19)$$

where $F : \mathbb{R}^k \rightarrow \mathbb{R}^k$ is a sufficiently smooth diffeomorphism.

F may represent, for example, the model of the virtual fly. If the target moves on a linear trajectory, the pursuer also flies along this direction and additionally performs complicated moves in order to catch the target. To analyze the occurrence of rigid trajectories and their stability, the movement along the linear trajectory is unimportant and for the analysis it is even disturbing, since fixed states cannot exist. A way out of this dilemma lies in a transformation into a comoving coordinate system. Formally, this can be archived as follows.

Denote by $\Gamma(u)$ some transformation, e.g. a rotation (where u is the angle, $u \in U = S^1 = \mathbb{R}/2\pi\mathbb{Z}$) or a translation (where u is the shift, $u \in U = \mathbb{R}^k$), fulfilling

$$\Gamma(u_2)\Gamma(u_1) = \Gamma(u_2 + u_1) \quad \text{for all } u_1, u_2 \in U. \quad (20)$$

Assume that the so called equivariance relation

$$F(\Gamma(u)x) = \Gamma(u)F(x) \quad (21)$$

holds for all $u \in U$, see [Chossat & Lauterbach, 2000, Golubitsky & Stewart, 2002]. Let $(u_n)_{n \in \mathbb{N}}$ be a sequence in U . Define a second dynamical system by

$$y_{n+1} = H(y_n) := F(\Gamma(u_{n+1})y_n), \quad n \in \mathbb{N}. \quad (22)$$

The following proposition shows that orbits of (22) can be transformed into orbits of the original system (19). Thus the two systems exhibit the same dynamical phenomena. Therefore, one chooses a transformation $\Gamma(u)$, fulfilling (20), such that that the system (22) is as simple as possible.

Proposition 2 *Let $(x_n)_{n \in \mathbb{N}}$ be an orbit of (19). Then*

$$y_n := \Gamma(u_n) \dots \Gamma(u_0)x_n, \quad n \in \mathbb{N}$$

defines an orbit of (22).

References

- Beyn, W.-J. and Thümmmler, V. [2004]. Freezing solutions of equivariant evolution equations. *SIAM J. Appl. Dyn. Syst.*, 3(2),85–116 (electronic).
- Böddeker, N. and Egelhaaf, M. [2003]. Steering a virtual blowfly: simulation of visual pursuit. *Proc. R. Soc. Lond. B*, pages 1971–1978.
- Böddeker, N. and Egelhaaf, M. [2005]. A single control system for smooth and saccade-like pursuit in blowflies. *Journal of Experimental Biology*, 208,1563–1572.
- Böddeker, N., Kern, R., and Egelhaaf, M. [2003]. Chasing a dummy target: smooth pursuit and velocity control in male blowflies. *Proc. R. Soc. Lond. B*, pages 393–399.
- Chossat, P. and Lauterbach, R. [2000]. *Methods in equivariant bifurcations and dynamical systems*, volume 15 of *Advanced Series in Nonlinear Dynamics*. World Scientific Publishing Co. Inc., River Edge, NJ.
- Collett, T. and Land, M. [1978]. How hoverflies compute interception courses. *J. Comp. Physiol. A*, 125,191–204.
- Dhooge, A., Govaerts, W., and Kuznetsov, Y. A. [2003]. MATCONT: a MATLAB package for numerical bifurcation analysis of ODEs. *ACM Trans. Math. Software*, 29(2),141–164.
- Golubitsky, M. and Stewart, I. [2002]. *The symmetry perspective*, volume 200 of *Progress in Mathematics*. Birkhäuser Verlag, Basel. From equilibrium to chaos in phase space and physical space.
- Hofbauer, J. and Iooss, G. [1984]. A Hopf bifurcation theorem for difference equations approximating a differential equation. *Monatsh. Math.*, 98(2),99–113.
- Hüls, T. [2005]. Instability helps virtual flies to mate. *Biol. Cybernet.*, 93(3),222–229.
- Hüls, T. [2007]. A model function for non-autonomous bifurcations of maps. *Discrete Contin. Dyn. Syst. Ser. B*, 7(2),351–363 (electronic).
- Kuznetsov, Y. A. [2004]. *Elements of Applied Bifurcation Theory*, volume 112 of *Applied Mathematical Sciences*. Springer-Verlag, New York, third edition.
- Land, M. and Collett, T. [1974]. Chasing behaviour of houseflies (*Fannia canicularis*). A description and analysis. *J. Comp. Physiol.*, 89,331–357.
- Langa, J. A., Robinson, J. C., and Suárez, A. [2006]. Bifurcations in non-autonomous scalar equations. *J. Differential Equations*, 221(1),1–35.
- Rasmussen, M. [2006]. Towards a bifurcation theory for nonautonomous difference equations. *J. Difference Equ. Appl.*, 12(3-4),297–312.
- Wiggins, S. [2003]. *Introduction to Applied Nonlinear Dynamical Systems and Chaos*, volume 2 of *Texts in Applied Mathematics*. Springer-Verlag, New York, second edition.